

Cryo-EM structures of intermediates suggest an alternative catalytic reaction cycle for cytochrome c oxidase

F. Kolbe^{1,4}, S. Safarian^{1,4}, Ž. Piórek^{1,3}, S. Welsch², H. Müller¹ & H. Michel¹✉

Cytochrome c oxidases are among the most important and fundamental enzymes of life. Integrated into membranes they use four electrons from cytochrome c molecules to reduce molecular oxygen (dioxygen) to water. Their catalytic cycle has been considered to start with the oxidized form. Subsequent electron transfers lead to the **E**-state, the **R**-state (which binds oxygen), the **P**-state (with an already split dioxygen bond), the **F**-state and the **O**-state again. Here, we determined structures of up to 1.9 Å resolution of these intermediates by single particle cryo-EM. Our results suggest that in the **O**-state the active site contains a peroxide dianion and in the **P**-state possibly an intact dioxygen molecule, the **F**-state may contain a superoxide anion. Thus, the enzyme's catalytic cycle may have to be turned by 180 degrees.

¹Department of Molecular Membrane Biology, Max Planck Institute of Biophysics, D-60438 Frankfurt/Main, Germany. ²Central Electron Microscopy Facility, Max Planck Institute of Biophysics, D-60438 Frankfurt am Main, Germany. ³Present address: Institute of Pharmaceutical Chemistry, Phillips University Marburg, D-35032 Marburg, Germany. ⁴These authors contributed equally: F. Kolbe, S. Safarian. ✉email: hartmut.michel@biophys.mpg.de

Cytochrome *c* oxidases (CcOs), members of the heme-copper superfamily of terminal oxidases, are among the most fundamental enzymes of life. Located in the inner membrane of mitochondria or of some prokaryotes they reduce molecular oxygen (dioxygen) to water and generate an electrochemical proton gradient across the membrane by using electrons from the external and protons from the internal membrane side as well as by proton pumping^{1–3}. In order to understand these processes, it is essential to know the structures of the intermediates of the catalytic cycle which comprises the oxidized form (O-state), the reduced CcO (R-state), the P-state (after reaction with dioxygen), then the F-state and again the O-state after successive electron transfers (Fig. 1).

In the conventional view (see Fig. 1) the reaction catalyzed by CcOs starts with electron transfer from a reduced cytochrome *c* to Cu_A. Electrons are subsequently transferred to the binuclear centre (BNC) via the low spin heme *a*. The BNC is composed of the high-spin heme *a*₃ and the Cu_B center and constitutes the active site of the enzyme^{4,5}. The oxidized BNC [O (Fe_{a3}³⁺, Cu_B²⁺)] is reduced by the first electron leading to the appearance of the E-state (E = electronated) which is converted to an R-state [R (Fe_{a3}²⁺, Cu_B⁺)] by further electron transfer. The R-state binds dioxygen forming compound A⁶. The original belief that two electrons are transferred onto the bound dioxygen creating a peroxide in the BNC, the P-state, (see e.g., ref. 7) has been challenged on the basis of the results of resonance Raman spectroscopy and magnetic circular dichroism spectroscopy^{8,9}. These results indicated that the dioxygen bond is already broken in the P-state, one oxygen atom has been bound to the heme *a*₃-Fe via a double bond, thus forming an oxoferryl moiety whereas the second oxygen atom is released as water. However, for the splitting of the dioxygen bond four electrons are required. Two of them would be provided by the heme *a*₃-Fe, one by Cu_B. The potential donors of the missing fourth electron are shown (Fig. 1). Currently, a tyrosine residue cross-linked to a histidine ligand of Cu_B is favored. A simultaneous transfer of four electrons onto

dioxygen is supposed to lead to the splitting of the dioxygen bond without the danger of forming reactive oxygen species. Whether a truly peroxidic P-state is part of the reaction cycle has been discussed controversially. Early Raman spectroscopy studies had suggested the presence of a peroxidic P-state intermediate while the later results have been interpreted in favor of the presence of an oxoferryl moiety in the BNC^{8–10}. The proposal that the P-state already contains an oxoferryl moiety has found rapid acceptance because Weng and Baker had claimed that the 606- (P-state) and 580 nm (F-state) species do not differ in oxidation state, and the F-state, obtained after the input of the third electron, is generally believed to contain an oxoferryl moiety¹¹. More recently there has been a comeback of a true peroxidic P-state intermediate¹². Input of the fourth electron leads to formation of a water molecule (or a hydroxide) closing the cycle.

In this work we used single-particle cryo-electron microscopy (cryo-EM) to determine high-resolution structures of biochemically defined and adjusted intermediate states (O, R, P_{CO} (carbon monoxide induced), F) of the wild type four-subunit CcO from *Paracoccus denitrificans* in lipid nanodiscs complexed with an Fv-antibody-fragment. These intermediate states refined locally to 1.9 Å (O), 2.6 Å (R), 1.9 Å (P_{CO}) and 2.3 Å (F) resolution. Our density maps provided insights into the active site configuration during the catalytic cycle revealing expected and unexpected rearrangements of dioxygen species in proximity to the BNC for the O, P, and F intermediates. In addition, we found densities for many dioxygen molecules in particular in the O-state CcO. Collectively, our results suggest that the established CcO catalytic cycle may have to be revised.

Results and discussion

We recorded UV/visible absorption spectra throughout the specimen preparation to confirm the presence of the desired specific electron-induced catalytic intermediate states (Fig. 2, Supplementary Fig. 1). The O-state CcO showed a Soret peak with an

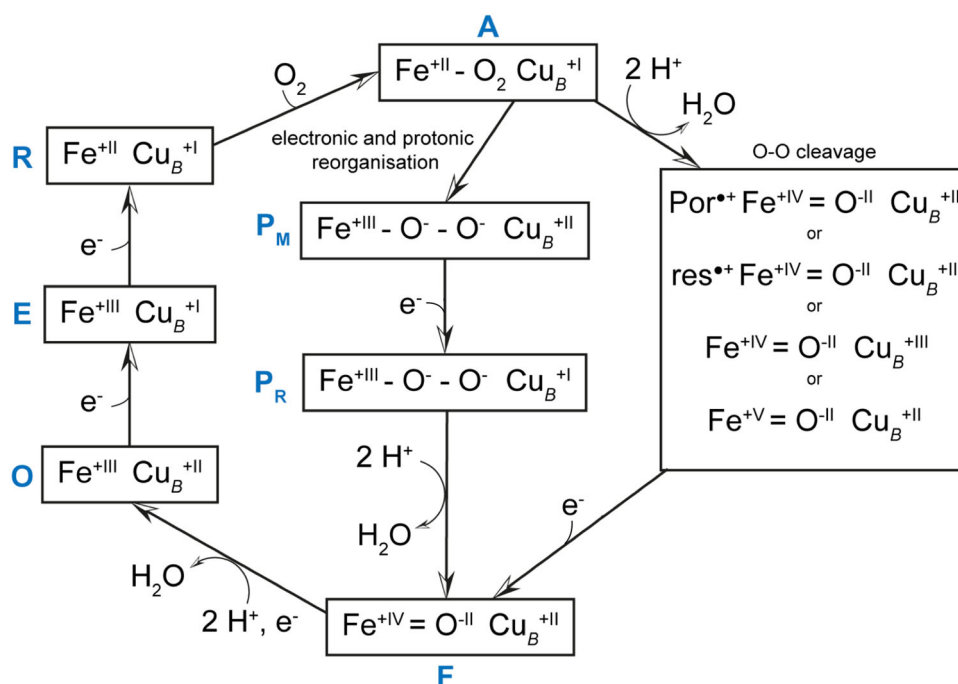


Fig. 1 The structure of oxygen intermediates in the catalytic cycle of cytochrome *c* oxidase. As the chemical composition of the P-state remains unsettled, alternative proposed structures are presented (intact dioxygen bond left, split bond right). Por[•] and res[•] denote radicals of the porphyrin ring and a spatially close amino acid residue, respectively.

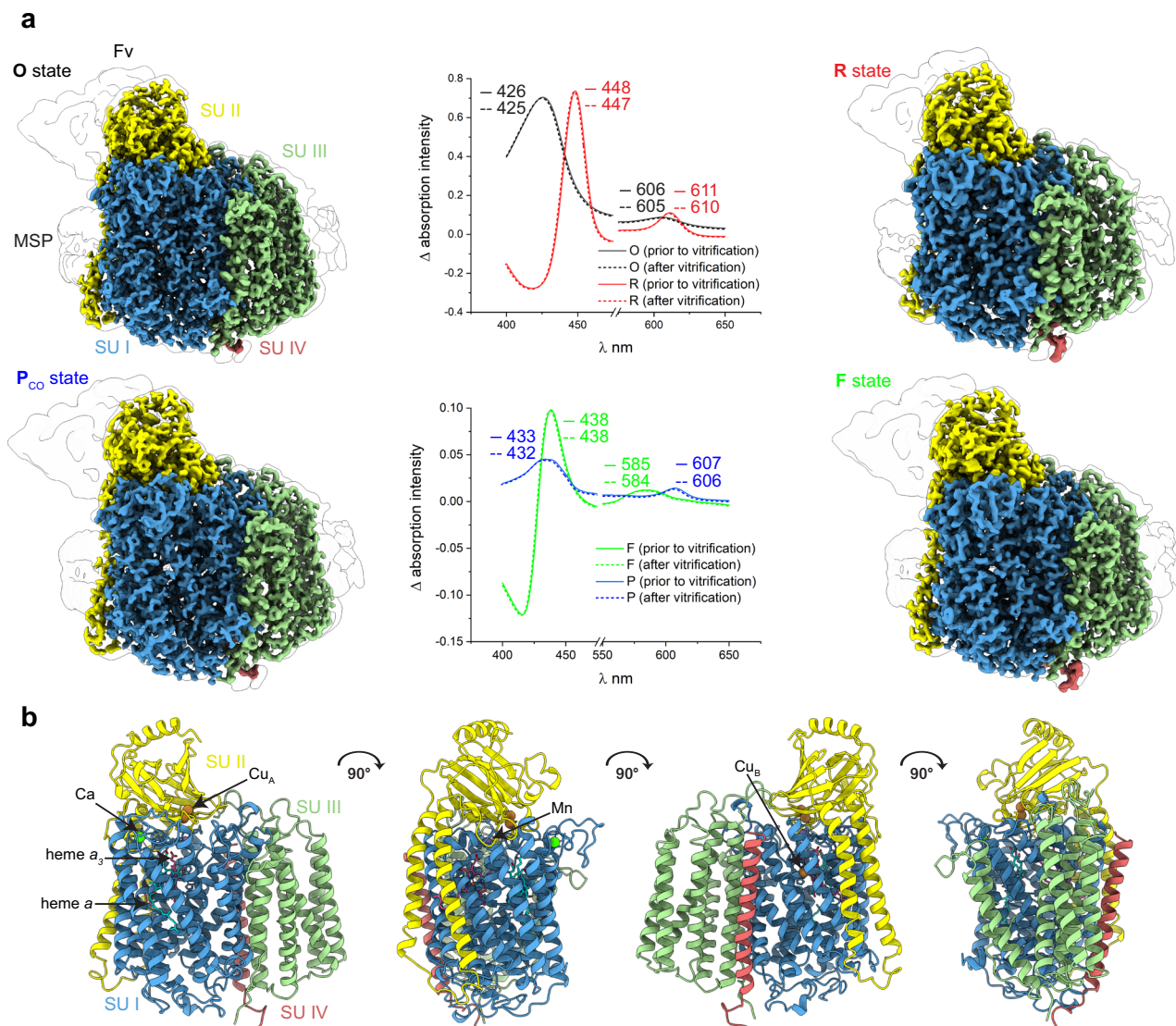


Fig. 2 Cryo-EM structure of the aa_3 CcO oxidase from *P. denitrificans*. **a** Surface representation of each intermediate state of the CcO at 1.9 Å (**O**), 2.6 Å (**R**), 1.9 Å (**P_{CO}**), and 2.3 Å (**F**) resolution. Uv/visible absorption spectra were individually and consistently recorded (intermediate state minus **O**-state). The illustrated map densities are filtered to equal contour levels of 1. **b** Ribbon representation of all four subunits with corresponding cofactors of the CcO. Color scheme: SU I, blue; SU II, yellow; SU III, green; SU IV, red. The antibody fragment (Fv) and membrane scaffold protein (MSP) are shown as a white surface.

absorption maximum at 426 nm, while that of the **R**-state is red-shifted to 448 nm. The difference absorption spectrum (**P_{CO}** minus **O**) for the two-electron induced **P_{CO}**-state ($\text{CO} + 2\text{OH}^- \rightarrow 2\text{e}^- + \text{CO}_2 + \text{H}_2\text{O}$) showed a Soret peak at 433 nm (α -band at 607 nm) which is distinct from the three electron-induced **F** state with its maximum at 438 nm (α -band at 585 nm).

Identification of the dioxygen channel. We start with a description of the **O**-state (Supplementary Fig. 2–7). Our density map allowed us to model a continuous cluster of dioxygen molecules, starting at the hydrophobic membrane interface near Val^{42.1} of TMH1.I and Leu^{149.1} of TMH3.I, ending at Val^{279.1} in proximity to the dioxygen binding site of heme a_3 and Cu_B (Fig. 3a/3b). Comparable corresponding densities were not observed for the fully reduced enzyme, however, they are in excellent agreement with the molecular dynamics results of Hofacker and Schulten¹³. We performed computational assisted calculations (MOLE 2.5¹⁴) to map possible channels within the **O**-state structure. We identified a continuous hydrophobic

pathway that overlaps with the densities assigned as oxygen molecules (Fig. 3c/3d). This pathway is in good agreement with the previously characterized oxygen channel of a B-type cytochrome *c* oxidase¹⁵. The entry site of our proposed channel is defined by a cavity at the interface between the transmembrane region and the hydrophobic membrane environment located in subunit I. Site-directed mutagenesis experiments have demonstrated a significantly higher K_M for oxygen when replacing Val^{279.1} by isoleucine^{16,17}. We conclude that impairment of oxygen binding and reduction in the V279I mutant is caused by the introduced bulky residue at the end of our identified oxygen channel restricting access to the dioxygen reduction site (Supplementary Fig. 8).

O-state. In the **O**-state structure, we were able to identify a prominent density within the binuclear center (BNC) between heme a_3 and Cu_B. Careful refinements with respect to distances to neighbouring molecules led to the assignment of a bridging peroxide species for this density in agreement with previous X-ray

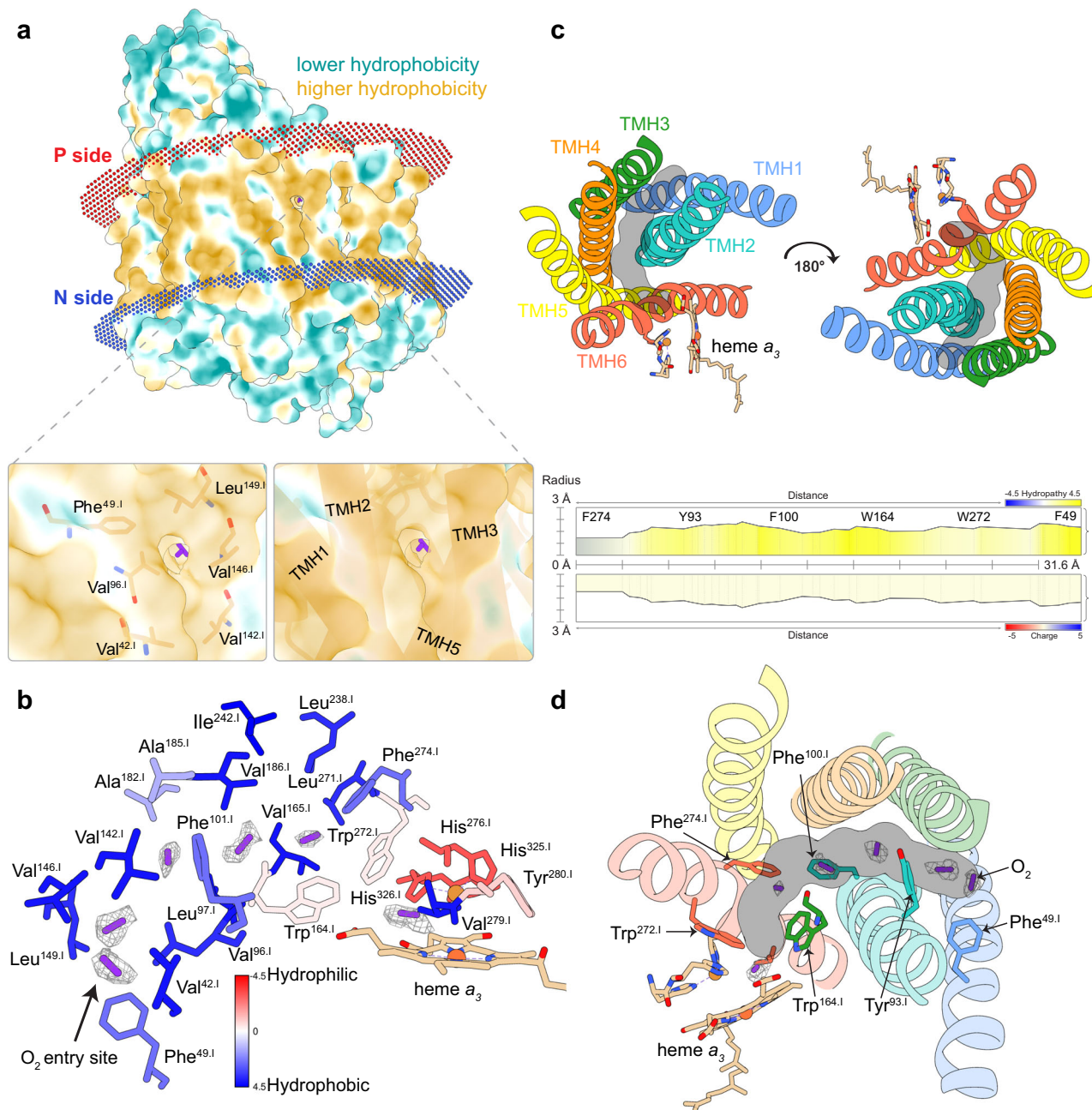


Fig. 3 Oxygen entry site and channel composition. **a** Surface representation of CcO and its oxygen entry point located between the transmembrane helix (TMH) 1 and 3 in the hydrophobic transmembrane site. The illustrated map density is filtered to a contour level of 2. **b** Detailed composition of the oxygen-conducting channel based on their hydrophobicity. The illustrated map density is filtered to a contour level of 0.5. **c** Interior channel embedded in between six transmembrane helices and channel lining residues predicted by Mole 2.5. **d** Overlay of channel prediction and individually displayed lining residues with corresponding di-oxygen densities. Di-oxygen molecules are shown as purple sticks, the corresponding densities are highlighted by mesh volumes.

structures (Fig. 4)^{18–22}. As previously outlined, more than 90 non-protein-derived peroxide structures that bridge two metal ions include an average length of $1.44 \pm 0.06 \text{ \AA}$ for the average O–O distance which is in accordance with our fitted peroxide dianion (1.42 \AA)²⁰. Neither a single nor two hydroxide ions could efficiently reside in this location since the density of one anion would be too weak while individual hydroxide ions couldn't be accommodated due to insufficient space in proximity to both metals. The Fe_{a_3} – Cu_B distance is 4.7 \AA with the heme a_3 iron (93°) coordinated almost in-plane to the porphyrin scaffold calculated from the merged bond angles heme a_3 N–Fe–His₄₁₁. The existence of peroxide in the BNC as observed in various X-ray structures

has not found much acceptance despite the fact that it has been shown that six electrons are required to fully reduce the as isolated oxidized CcO^{18,21,23}. Four electrons would be needed to reduce the four prosthetic groups of CcO and two to reduce the peroxide. A peroxide bridge would be ideally suited to electrostatically compensate the positive charges at Fe_{a_3} and Cu_B . The peroxide has been claimed to be an artifact of X-ray radiation by X-ray induced reduction of di-oxygen molecules present in the crystals^{21,23,24}. The observation of a density for a di-oxygen molecule, presumably peroxide, by cryo-EM definitely rules out such explanations. In close proximity to the peroxide dianion (3 \AA), we observed a distinct density feature which most likely represents a

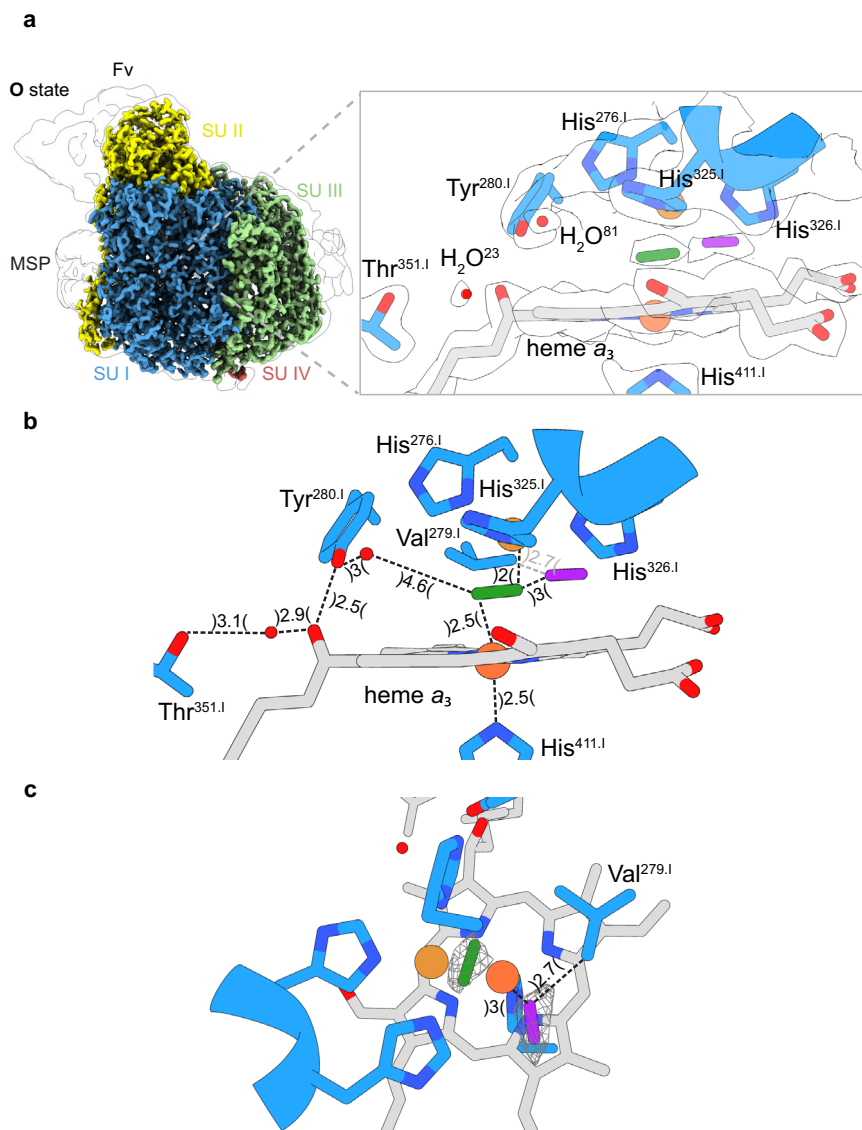


Fig. 4 Cryo-EM density map (**O**-state) and modelled structure of the binuclear site in CcO. **a** Structural overview of the binuclear site in the **O**-state. The bridging peroxide species (green) is located in-between the iron (orange) and the copper (brown) atom. In close proximity to the observed bridging ligand, a second prominent density presumably molecular oxygen (purple), is located. **b** Measured distances (Å) for the modelled molecules at the active site. **c** Top view of the active site. The corresponding density map is illustrated as a white surface or mesh volumes. The illustrated map densities are filtered to equal contour levels of 1.5.

dioxygen molecule bound near Val^{279.1} (2.7 Å). This resting oxygen molecule is located at the end of the identified substrate conducting channel presented above.

R-state. The structure of the fully reduced **R**-state CcO does not show any density between Fe_{a3} and Cu_B nor does it show densities for bound oxygen in the substrate conducting channel (Fig. 5). The absence of the densities assigned to dioxygen molecules in the **O**-state after the dithionite treatment supports the assignment of the observed densities in the channel of the **O**-state to dioxygen molecules. An interesting distinction between the **O**-state and the **R**-state is the different side-chain orientation of the prominent residue Lys^{354.1} of the K-pathway (Fig. 6). In the fully reduced **R**-state the side chain is found closer to the then more negatively charged BNC that might indicate that the lysine side chain is protonated, or becomes protonated during reduction. Figure 6 also presents the water molecules which form part of the proton transfer network and of the pump loading site.

P-state. **P**-states can be induced by a number of different methods²⁵. We chose to generate the **P**-state by limited exposure to carbon monoxide in the presence of oxygen thus denoted here as **P**_{CO}-state. This is a classical procedure discovered by Peter Nicholls and was used also in previous experiments^{25,26}. The presence of the **P**_{CO}-state was unambiguously confirmed by uv/vis spectroscopy. The structure in and around the BNC, obtained at a local resolution of sub 2 Å, met us with a big surprise. We identified a specific density between the two metal centers of the active site while, compared to the **O**-state, the nearby dioxygen molecule appears to be absent and to be replaced by a water molecule or a hydroxide ion (Fig. 7). The density map indicates the presence of a diatomic species, most likely with an intact O-O bond in the **P**_{CO}-state. Based on the location of this density and due to geometrical and steric restraints, we can exclude the presence of an oxoferryl heme species, and of a hydroxide ion or water bound to Cu_B (Cu_B – OH⁻/H₂O) suggested by previous studies. The two oxygen atoms would come too close. The

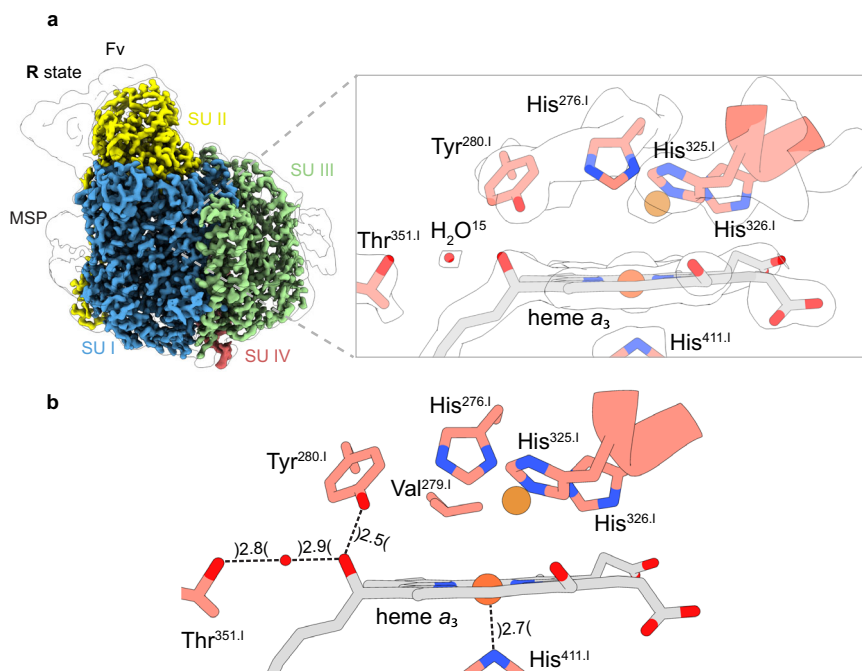


Fig. 5 Cryo-EM density map (R-state) and modelled structure of the binuclear site in CcO. a Structural overview of the binuclear site in the R-state. Densities located between the iron (orange) and copper atom (brown) were not observed, indicating a fully reduced binuclear site. **b** Measured distances (Å) for the modelled molecules at the active site. The corresponding density map is illustrated as a white surface. The illustrated map densities are filtered to equal contour levels of 1.5.

interatomic Fe-Cu_B distance is 4.7 Å while the heme a₃ iron remains almost in the plane with the ring system. The overall similarity to the O-state is extreme with the exception of the crosslink distance N_{e2}-His^{276.1} - C_{e2}-Tyr^{280.1}, decreasing from 2.3 Å (O) to 1.6 Å (P). Movements of the related helices are not observed (Supplementary Fig. 9). The density for the diatomic species in the P-state appears to be more parallel to the heme a₃ macrocycle than in the O-state. As outlined above the view based on resonance Raman spectroscopy that the dioxygen double bond has been already broken in the P-state appears to be widely accepted. However, one has to note that the species providing the signal in Raman spectroscopy may not reflect the most abundant population in the sample²⁷. In contrast, particle averaging and class sorting in cryo-EM result in weighted map densities with the most populated species having the strongest contribution to the map features.

What about the chemical experiment providing evidence for a split dioxygen bond in P_{CO}-state? There, the P_{CO}-state was generated by flashing off carbon monoxide from mixed-valence CO bound CcO in the presence of ¹⁸O₂. Approximately half of the ¹⁸O-label, compared to the amount of P_{CO}-state CcO, was found as water²⁸. However, the reaction of CO with dioxygen yielding CO₂ and water would provide the same experimental result.

What then can be the nature of the diatomic species between the two metals of the BNC? We can exclude carbon monoxide on the basis of the spectroscopic features of the state generated and investigated. A peroxide dianion would be a possibility. However, the BNC of the O-state contains two electrons more than that of the P_{CO}-state (see Fig. 1). If one accepts that the O-state BNC contains a peroxide dianion, the BNC of P_{CO}-state should contain a neutral dioxygen molecule! In agreement with this proposal, quantum chemical calculations have indicated that binding of dioxygen to the oxidized BNC is energetically favorable²³.

F-state. In order to gain insights into the previously unknown ligand arrangement of the F-state BNC, we treated the CcO with an excess of hydrogen peroxide as published²⁵. We obtained the structure of the F-intermediate at a resolution of 2.3 Å. The space between Cu_B and heme a₃ does not contain a distinct density (see Fig. 8) as observed for the P_{CO} state (Fig. 7). Hence, the absence of a dioxygen species is apparent. Based on the expectations we modelled a geometrically optimized oxoferryl group in the center of heme a₃ in agreement with previously postulated structures, despite the fact, that established X-ray crystallographically determined electron densities of oxoferryl heme moieties in proteins reveal a much better shape for the oxoferryl moiety²⁹. However, modeling simply a ferric iron into the central heme a₃ density is at least equally well possible (Fig. 8d). Modelling of a water molecule as a potential fourth Cu_B ligand, providing a hydrogen bond to the oxoferryl oxygen, was not possible because of insufficient space. The Fe_{a3}-Cu_B distance of 4.5 Å is similar to that in the O/P_{CO} state while the coordinated iron is slightly more displaced from the center of the heme macrocycle (95°) compared to the O state (93°). Furthermore, the cross-linked His^{276.1} - Tyr^{280.1} distance has increased by more than 1 Å (2.7 Å) compared to the P_{CO} state (1.6 Å). Clearly, the covalent crosslink between the N_{e2} of His^{276.1} and C_{e2} of Tyr^{280.1} appears to be subject of structural rearrangements based on the interatomic distance. This observation also means that a reinvestigation of whether the crosslink is opened in the F-state is required. In addition, the bonding distance between His^{411.1} - Fe_{a3} is shortened by ~0.3 Å (2.2 Å) which can be explained by a different protonated state as outlined previously³⁰. Intriguingly, a prominent and undescribed density is located between His^{326.1} and Val^{279.1} in close proximity to Cu_B (3.3 Å). Its shape and location argue for a dioxide species, dioxygen or superoxide. After reduction the latter could form a peroxide bridge between Fe_{a3} and Cu_B as observed in the O-state. We find a similar but slightly more displaced density also in the O-state in proximity to Val^{279.1}.

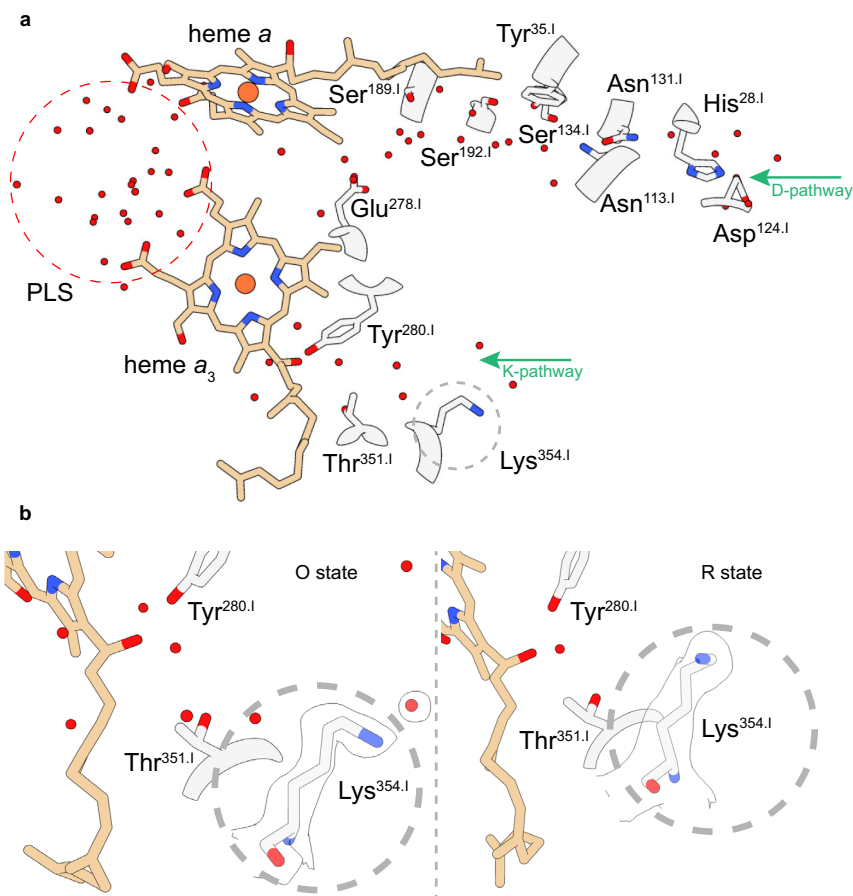


Fig. 6 Proton transfer pathways in CcO. **a** A structural overview of the two proton transfer pathways. The K and D-pathway are defined by their respective amino acids. Several water molecules could be assigned in each pathway and an accumulated water cluster could be seen near the A-ring propionate of heme a_3 , presumably the proton-loading site (PLS). **b** A redox-dependent positional change of the side chain of the key residue Lys^{354.1}, located in the K-pathway, was observed. It looks as the reduction of the BNC leads to an electrostatic attraction of the potentially positively charged side chain of Lys^{354.1}. The corresponding density map is illustrated as a white surface. Illustrated map densities are filtered to equal contour levels of 1.

in a more distant position (~ 0.4 Å, 3.7 Å) towards the Cu_B. The presence of superoxide at this position in the F-state agrees well with complementary EPR and ligand-mimicking studies, which have shown that treatment of the F-state CcO with catalase leads to an O-state like UV/vis spectrum and the appearance of a tyrosine radical²⁵. This observation can be explained if a superoxide present takes an electron from the CcO thus being converted to a peroxide that leaves the enzyme and is split by the catalase.

As mentioned above and presented in Fig. 8, modelling of the central density of heme a_3 iron as a ferric iron atom is at least equally well possible. The experimental result mentioned above that treatment of the F-state CcO with catalase leads to the formation of a CcO form with UV/vis spectral properties very similar to the O-state²⁵. The only difference to the O-state spectrum is the appearance of a broad absorption band around 630 nm. This band has been considered to be a charge transfer band of the ferric heme a_3 iron³¹. How could the simple addition of catalase lead to the removal of an oxygen atom from a central ferryl iron? We also would like to remind the reader of the postulate by Weng and Baker that the 606- (P-state) and 580 nm (F-state) species do not differ in oxidation state¹¹.

The scenario which fits our experimental results best is the following: The classical P-state is an oxygenated oxidized form of CcO. Upon reduction of the bound dioxygen by one electron a superoxide anion is formed which is observed near Cu_B. This form corresponds to the classical F-state. Upon input of another

electron, the superoxide is reduced to a peroxide, leading to the O-state with the peroxide bridging the heme a_3 iron and Cu_B.

For a complete cycle (Fig. 9) the observed O-state has to be reduced by two more electrons which would lead to the formation of two water molecules (or one water molecule and one hydroxide ion) which would have to be replaced by a dioxygen molecule forming the P-state again. We look with great interest into the structure determination of the one-electron reduced E-state.

Methods

Production of cytochrome c oxidase from *Paracoccus denitrificans*. The cytochrome c oxidase (cytochrome aa_3) from *Paracoccus denitrificans* was produced in *P. denitrificans* AO1 cells transformed with the pUB39 (pBBR1 MCS derivative) plasmid and RP-4 helper strain via triparental mating according to a standardized in-house protocol^{32,33}. A pre-culture was set up by adding 0.1 ml of 50% glycerol stock to 50 ml succinate (25 µg/ml kanamycin, 25 µg/ml streptomycin) growth medium. Cells were incubated at 32 °C while shaking (180 rpm) overnight. An intermediate-culture was started by inoculating 500 ml succinate (25 µg/ml kanamycin, 25 µg/ml streptomycin) growth medium with 50 ml of the pre-culture. Subsequently, cell production was carried out by growing the main culture with 2.5 l by adding 200 ml from the intermediate-culture at 32 °C while shaking (150 rpm) for approximately 8 hours. After harvest and homogenization, cells were disrupted using a high-pressure homogenizer (Constant Systems Ltd.) with an applied pressure of 25 kpsi. The cell lysate was centrifuged at $6,000 \times g$ at 4 °C for 60 min followed by an ultra-centrifugation step with a speed of $205,000 \times g$ at 4 °C for 12 h. Collected membrane pellets were suspended in 50 mM KPi (pH 8) with a concentration of 20 mg/ml.

Production and purification of the antibody-fragment from *E. coli* JM83 pASK68. The antibody-fragment Fv7E2 was produced in *E. coli* JM83 with the

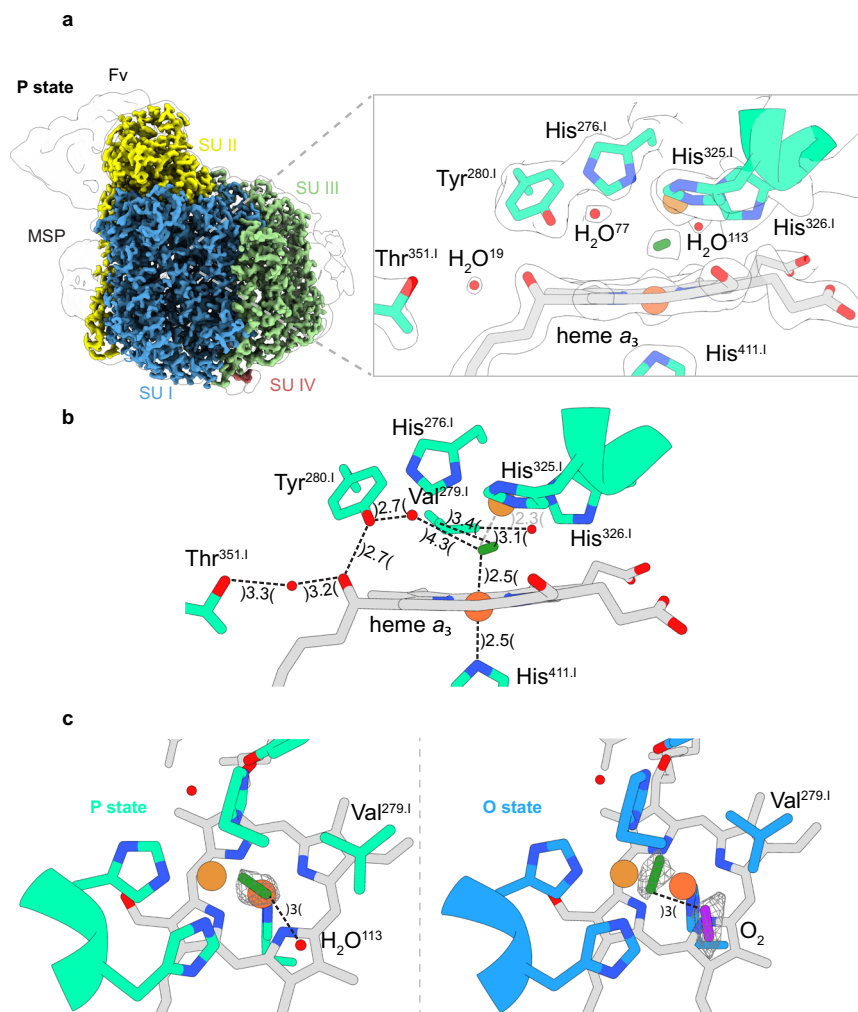


Fig. 7 Cryo-EM density map (P-state) and modelled structure of the binuclear site in CcO. **a** Structural overview of the binuclear site in the **P**-state. The bridging dioxygen ligand (green) is embedded between the iron (orange) and the copper (brown) atom. The previously observed dioxygen molecule in the **O**-state near Val^{279.1} is replaced by a water (H₂O¹¹³). **b** Measured distances (Å) for the modelled molecules at the active site. **c** Top view of the binuclear center of the **O** and **P**-state to illustrate the rotation of the bridging dioxygen species. The corresponding density map is illustrated as a white surface or mesh volumes. Illustrated map densities are filtered to equal contour levels of 1.5.

plasmid pASK68 which possess the ability to bind to SU II of CcO and carries a C-terminal Strep-tag^{34,35}. For production, a pre-culture was inoculated with a volume of 0.1 ml 50% glycerol stock and grown in a 200 ml LB (100 µg/ml ampicillin) growth medium at 30 °C (180 rpm) overnight. The 2 L main culture (100 µg/ml ampicillin) was grown at 23.5 °C while shaking (165 rpm) to an OD₆₀₀ of 0.5 before recombinant antibody-fragment production was induced by the addition of 0.5 mM IPTG for additional 3 h. Collected cell material was centrifuged at 3500 × g for 15 m at 4 °C and pellets were subsequently mixed with 500 mM sucrose, 35 mM KPi (pH 8) for 20 m on ice. The disrupted cell lysate was centrifuged at 24,000 × g at 4 °C for 60 m and the supernatant was collected.

Purification of cytochrome c oxidase from *P. denitrificans*. For preparation of the four-subunit cytochrome *c* oxidase, pelleted membranes were solubilized at pH 8 with 1 % dodecyl-β-maltoside (DDM) with a resulting mass ratio of 1 mg detergent per 5 mg of membrane proteins. In a first step, solubilized CcO was incubated with the strep-tagged Fv fragment for 30 min at 4 °C while stirring to allow efficient binding. Final mixture was centrifuged at 235,000 × g for 60 m at 4 °C and the supernatant was loaded on a Strep-Tactin[®] XT Superflow[®] high capacity column (IBA GmbH) to perform affinity chromatography. For washing during purification, 5 column volumes [CV] (50 mM KPi pH 8, 0.05% DDM) were used and for the final elution (5 CV), the washing buffer was supplemented with 50 mM biotin. To increase sample homogeneity, ion-exchange chromatography was performed using a Q Sepharose[®] High-Performance column (Sigma Aldrich). Two steps of washing containing 50 mM/200 mM KPi (pH 8), 0.05% DDM were performed before eluting with 300 mM KPi (pH 8) and 0.05% DDM. As a final sample polishing step, size exclusion chromatography was done using a Superdex 200 10/300 increase column (GE Healthcare Life Sciences) with a running buffer

consisting of 50 mM KPi (pH 8) and 0.02% DDM. Each purification was done in the presence of K₃[Fe(CN)₆] to keep the redox state of the cytochrome *c* oxidase consistent.

Production and purification of MSP1D1. The production of the N-terminal 7x histidine-tagged MSP1D1 (Membrane scaffold protein) was done according to a standardized protocol³⁶. Therefore, BL21Gold (DE3) *E. coli* cells were transformed with pMSP1D1 and grown in LB-Kan medium (50 µg/ml kanamycin) at 37 °C. By reaching an OD₆₀₀ of 0.6, induction with 1 mM IPTG was carried out to start the MSP1D1 production for 4 h before cell harvest. The pellet from 4 L cell culture was resuspended in a cell disruption buffer (20 mM Tris-Cl pH 8, 1 mM PMSF) and afterwards supplemented with Triton X-100 (1% (v/v)). The resulting lysate was centrifuged and filtered. In a final step, the cell solution was supplemented with 500 mM NaCl. The lysate was mixed with 6 mL Ni-NTA agarose (Thermo Fisher) which had been equilibrated with the washing buffer (20 mM Tris-Cl pH 8, 500 mM NaCl, 1% Triton X-100). The mixture was incubated for 12 hours while stirring at 4 °C. Next, the solution was loaded, washed and eluted with 500 mM imidazole. Eluted fractions were pooled and dialyzed against buffer (20 mM Tris-Cl, pH 7.5, 150 mM NaCl) and finalized samples were concentrated to 5 mg/mL, frozen in liquid nitrogen and stored at -80 °C.

Reconstitution of cytochrome c oxidase in MSP1D1 and lipids. The reconstitution of cytochrome *c* oxidase into lipid nanodiscs was accomplished by using the aforementioned protocols³⁶. Here, mixing POPC, MSP1D1 and the CcO was done in a molar ratio of 500:10:1 and subsequently incubated at 4 °C for 1 h. Detergent removal from the mixture was conducted by adding three times 0.2 mg dried Bio-Beads[™] SM-2 (Bio-Rad) every 2 h keeping at 4 °C. For successful

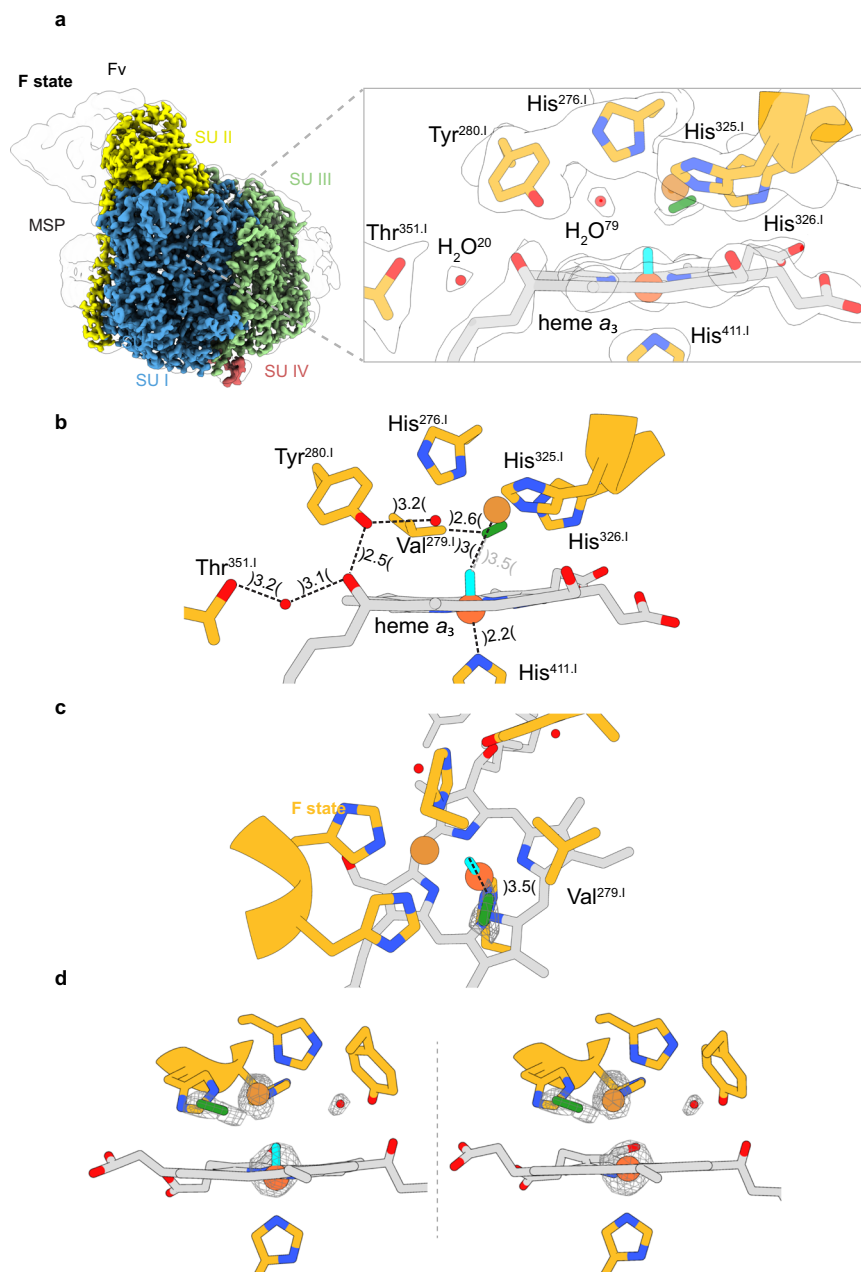


Fig. 8 Cryo-EM density map (F-state) and modelled structure of the binuclear site in CcO. **a** Structural overview of the binuclear site in the F-state. No bridging ligand is located between the iron (orange) and the copper (brown) atom. Instead, the density map may indicate the presence of an oxoferryl (cyan) at the heme and a dioxide species (green) in close proximity. **b** Measured distances (Å) for the modelled molecules at the active site. **c** Top view of the binuclear center of the F-state. **d** Modeling of the iron of heme a_3 with a bound oxygen (oxoferryl) and without. The corresponding density map is illustrated as a white surface or mesh volumes. Illustrated map densities are filtered to equal contour levels of 1.5.

formation, the mixture was incubated for an additional 12 h at 4 °C while shaking. Removal of Bio-Beads was done by filtration and the reconstituted CcO was applied to a Superdex 200 10/300 increase column to exclude empty nanodiscs using 50 mM KPi (pH 8) as a final buffer. Fractions containing nanodisc-reconstituted aa_3 oxidase were pooled together, concentrated to 2 mg/ml and directly used for subsequent cryo-EM experiments.

Optical spectroscopy. To establish a defined ground state with an Soret maximum around 425 nm, the protein was fully oxidized during the size exclusion chromatography step in the presence of 200 μ M $K_3[Fe(CN)_6]$. UV/visible absorption spectra of each state were recorded using a PerkinElmer Lambda 35 UV/visible spectrophotometer. Different biochemical defined states (R, P, F) were set according to a given in-house method with slight adjustments²⁵. 50 mM KPi (pH 8) was mixed with 2 mg/ml (~12 μ M) of reconstituted CcO in a quartz cuvette with 1 cm path length. To prepare the artificial intermediates P_{CO} and F, the

reconstituted CcO was either incubated with CO (Air Liquid Deutschland GmbH) aerobically for 15 m on ice while stirring (P_{CO}) or mixed with H_2O_2 in 1:500 molar ratio (F). Full reduction (R) of the protein mixture was achieved by adding stoichiometric amounts of sodium dithionite. To confirm the presence of each electron-induced state, UV/visible absorption spectra were recorded prior to sample vitrification and afterwards for each cryo-EM experiment from the same protein batch. From sample adjustment to freezing in liquid ethane, no more than 10 m were used to avoid potential decay processes.

Single-particle cryo-electron microscopy

Sample vitrification. Quantifoil R1.2/1.3 copper grids (mesh 200) were firstly washed with chloroform and then glow discharged twice with a PELCO easiGlow device at 15 mA for 45 s. For each recorded data set, a volume of 4 μ l protein sample (2 mg/ml) was applied on the grid before plunge freezing. Samples were vitrified at 4 °C, 100% humidity, and a blot force of 20 using a Vitrobot IV device

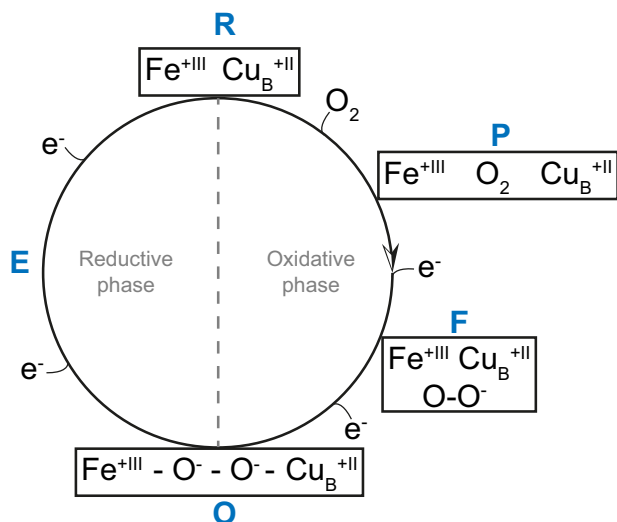


Fig. 9 A potential catalytic cycle of CcO based on our results. The classical **P**-state is an oxygenated oxidized form of CcO. Input of one electron reduces the bound dioxygen to superoxide which remains bound in the BNC near Cu_B (classical **F**-state). Input of another electron reduces the superoxide to a peroxide which forms a bridging ligand in the BNC of the **O**-state. The next input of an electron leads to the formation of the classical **E**-state whose structure is still unknown. Input of the fourth electron leads to the formation of a 2-electron **R**-state which binds a dioxygen molecule closing the cycle. Two water molecules or one water molecule plus one hydroxide ion are formed during the input of the third and fourth electrons in the classical reductive phase.

(Thermo Fisher Scientific). The blotting time was set to 4 s before plunge freezing in liquid ethane.

Image recording. Images for each data set were recorded by using a Titan Krios G3 microscope operated at 300 kV (Thermo Fisher Scientific). Coma and beam tilt correction was done by using EPU (Thermo Fisher Scientific) and data collection was conducted by operating in an electron counting mode with a Falcon III direct electron detector at a nominal magnification of $\times 96,000$, corresponding to a calibrated pixel size of 0.833 Å. An accumulated dose of $0.98 \text{ e}^-/\text{Å}^2$ per fraction was used for the 30 dose-fractionated frames (\sim total dose $30 \text{ e}^-/\text{Å}^2$). Defocus values were applied in a range from 0.5 to 2.5 μm .

Image processing. Collected data in MRC format were consistently processed with RELION-3.1^{37,38} and motion-corrected with the MotionCor2 algorithm³⁹. Initial CTF parameters from each dose-weighted image were determined by using CTFIND4⁴⁰ and particle images were automatically selected followed by initial model building, 3D classification, CTF refinement, Bayesian polishing and final map reconstruction using RELION-3.1. Unfiltered maps were sharpened by applying different b-factors for building and visual improvement purposes. The final overall resolution was estimated by using the gold-standard Fourier shell correlation ($\text{FSC}_{0.143}$) which was calculated from two independently refined data sets. Global resolution anisotropy was examined by RELION-3.1. Observable map quality improvements were achieved by applying a density-modification procedure to each data set in a consistent way⁴¹. For this purpose, both half maps and a sequence file were used together with a model file, a full map file and a mask file. Significant map improvements were already observed after one cycle and were repeated until no further improvement was observed (Supplementary Figs. 2–7).

Model building and geometry refinement. For building the four-subunit atomic model of the cytochrome aa_3 oxidase, the Protein Data Bank (PDB) submission by Harrenga et al. (PDB 1QLE) was used as a template structure⁴². After manual backbone fitting and correct fitting of side chains in the respective map densities, real-space refinement was done using Phenix (version 1.18)⁴³. As a final building step, density-modified maps were used for more precise molecule allocation around the catalytic center. Each finalized model was validated by the MolProbity online server⁴⁴. A final summary for each model parameter and its corresponding cryo-EM statistics can be found in Supplementary Table 1. Finalized models were visualized by using Chimera⁴⁵ and ChimeraX⁴⁶.

Visualization of an oxygen channel. The proposed oxygen channel was mapped with MOLE 2.5 (bottleneck radius: 1.5 Å, bottleneck tolerance 3 Å, origin radius 5 Å, surface cover radius 10 Å, max tunnel similarity 1)¹⁴ and visualized with Chimera. Oxygen molecules were manually placed with Coot into corresponding densities observed in the O-state map.

Reporting Summary. Further information on research design is available in the Nature Research Reporting Summary linked to this article.

Data availability

The generated cryo-EM maps of the aa_3 cytochrome c oxidase from *Paracoccus denitrificans* have been deposited at the Electron Microscopy Data Bank under accession codes EMD-11921, EMD-11922, EMD-11924 and EMD-11925. The models of the aa_3 cytochrome c oxidase structures were submitted to the PDB data bank with the accession numbers: 7ATE, 7AU6, 7ATN, and 7AU3. 1QLE was used as a template. All other data is presented in the main text or supplementary information.

Received: 9 July 2021; Accepted: 29 October 2021;

Published online: 25 November 2021

References

- Wikstrom, M. K. Proton pump coupled to cytochrome c oxidase in mitochondria. *Nature* **266**, 271–273 (1977).
- Michel, H., Behr, J., Harrenga, A. & Kannt, A. Cytochrome c oxidase: structure and spectroscopy. *Annu Rev. Biophys. Biomol. Struct.* **27**, 329–356 (1998).
- Brzezinski, P. Redox-driven membrane-bound proton pumps. *Trends Biochem Sci.* **29**, 380–387 (2004).
- Richter, O. M. & Ludwig, B. Electron transfer and energy transduction in the terminal part of the respiratory chain - lessons from bacterial model systems. *Biochim Biophys. Acta.* **1787**, 626–634 (2009).
- Yoshikawa, S. & Shimada, A. Reaction mechanism of cytochrome c oxidase. *Chem. Rev.* **115**, 1936–1989 (2015).
- Chance, B., Saronio, C. & Leigh, J. S. Jr. Functional intermediates in the reaction of membrane-bound cytochrome oxidase with oxygen. *J. Biol. Chem.* **250**, 9226–9237 (1975).
- Babcock, G. T. & Wikstrom, M. Oxygen activation and the conservation of energy in cell respiration. *Nature* **356**, 301–309 (1992).
- Fabian, M. & Palmer, G. The interaction of cytochrome oxidase with hydrogen peroxide: the relationship of compounds P and F. *Biochemistry* **34**, 13802–13810 (1995).
- Ogura, T. & Kitagawa, T. Resonance Raman characterization of the P intermediate in the reaction of bovine cytochrome c oxidase. *Biochim Biophys. Acta.* **1655**, 290–297 (2004).
- Varotsis, C., Zhang, Y., Appelman, E. H. & Babcock, G. T. Resolution of the reaction sequence during the reduction of O_2 by cytochrome oxidase. *Proc. Natl Acad. Sci. USA* **90**, 237–241 (1993).
- Weng, L. C. & Baker, G. M. Reaction of hydrogen peroxide with the rapid form of resting cytochrome oxidase. *Biochemistry* **30**, 5727–5733 (1991).
- Poiana, F. et al. Splitting of the O-O bond at the heme-copper catalytic site of respiratory oxidases. *Sci. Adv.* **3**, e1700279 (2017).
- Hofacker, I. & Schulten, K. Oxygen and proton pathways in cytochrome c oxidase. *Proteins* **30**, 100–107 (1998).
- Pravda, L. et al. MOLEonline: a web-based tool for analyzing channels, tunnels and pores (2018 update). *Nucleic Acids Res.* **46**, W368–W373 (2018).
- Luna, V. M., Chen, Y., Fee, J. A. & Stout, C. D. Crystallographic studies of Xe and Kr binding within the large internal cavity of cytochrome ba_3 from *Thermus thermophilus*: structural analysis and role of oxygen transport channels in the heme-Cu oxidases. *Biochemistry* **47**, 4657–4665 (2008).
- Riistama, S. et al. Channelling of dioxygen into the respiratory enzyme. *Biochimica et Biophysica Acta (BBA) - Bioenerg.* **1275**, 1–4 (1996).
- Riistama, S., Puustinen, A., Verkhovsky, M. I., Morgan, J. E. & Wikstrom, M. Binding of O_2 and its reduction are both retarded by replacement of valine 279 by isoleucine in cytochrome c oxidase from *Paracoccus denitrificans*. *Biochemistry* **39**, 6365–6372 (2000).
- Aoyama, H. et al. A peroxide bridge between Fe and Cu ions in the O_2 reduction site of fully oxidized cytochrome c oxidase could suppress the proton pump. *Proc. Natl. Acad. Sci. USA* **106**, 2165–2169 (2009).
- Qin, L., Hiser, C., Mulichak, A., Garavito, R. M. & Ferguson-Miller, S. Identification of conserved lipid/detergent-binding sites in a high-resolution structure of the membrane protein cytochrome c oxidase. *Proc. Natl. Acad. Sci. USA* **103**, 16117–16122 (2006).
- Koepke, J. et al. High resolution crystal structure of *Paracoccus denitrificans* cytochrome c oxidase: New insights into the active site and the proton transfer

- pathways. *Biochimica et Biophysica Acta (BBA) - Bioenerg.* **1787**, 635–645 (2009).
21. Tiefenbrunn, T. et al. High resolution structure of the ba3 cytochrome c oxidase from *Thermus thermophilus* in a lipidic environment. *PLoS One* **6**, e22348 (2011).
 22. Ishigami, I. et al. Snapshot of an oxygen intermediate in the catalytic reaction of cytochrome c oxidase. *Proc. Natl. Acad. Sci. USA* **116**, 3572–3577 (2019).
 23. Kaila, V. R. et al. A combined quantum chemical and crystallographic study on the oxidized binuclear center of cytochrome c oxidase. *Biochim Biophys. Acta.* **1807**, 769–778 (2011).
 24. Andersson, R. et al. Serial femtosecond crystallography structure of cytochrome c oxidase at room temperature. *Sci. Rep.* **7**, 4518 (2017).
 25. von der Hocht, I. et al. Interconversions of P and F intermediates of cytochrome c oxidase from *Paracoccus denitrificans*. *Proc. Natl. Acad. Sci. USA* **108**, 3964–3969 (2011).
 26. Nicholls, P. A new carbon monoxide-induced complex of cytochrome c oxidase. *Biochem. J.* **175**, 1147–1150 (1978).
 27. Ferguson-Miller, S. & Babcock, G. T. Heme/Copper Terminal Oxidases. *Chem. Rev.* **96**, 2889–2908 (1996).
 28. Fabian, M., Wong, W. W., Gennis, R. B. & Palmer, G. Mass spectrometric determination of dioxygen bond splitting in the “peroxy” intermediate of cytochrome c oxidase. *Proc. Natl. Acad. Sci. USA* **96**, 13114–13117 (1999).
 29. Gumiero, A., Metcalfe, C. L., Pearson, A. R., Raven, E. L. & Moody, P. C. Nature of the ferryl heme in compounds I and II. *J. Biol. Chem.* **286**, 1260–1268 (2011).
 30. Pinakoulaki, E. et al. The protein effect in the structure of two ferryl-oxo intermediates at the same oxidation level in the heme copper binuclear center of cytochrome c oxidase. *J. Biol. Chem.* **288**, 20261–20266 (2013).
 31. Morgan, J. E., Verkhovskiy, M. I., Puustinen, A. & Wikstrom, M. Identification of a “peroxy” intermediate in cytochrome bo3 of *Escherichia coli*. *Biochemistry* **34**, 15633–15637 (1995).
 32. Gerhus, E., Steinrucke, P. & Ludwig, B. *Paracoccus denitrificans* cytochrome c1 gene replacement mutants. *J. Bacteriol.* **172**, 2392–2400 (1990).
 33. Hilbers, F., von der Hocht, I., Ludwig, B. & Michel, H. True wild type and recombinant wild type cytochrome c oxidase from *Paracoccus denitrificans* show a 20-fold difference in their catalase activity. *Biochim. Biophys. Acta.* **1827**, 319–327 (2013).
 34. Kleymann, G., Ostermeier, C., Ludwig, B., Skerra, A. & Michel, H. Engineered Fv fragments as a tool for the one-step purification of integral multisubunit membrane protein complexes. *Biotechnol. (N. Y.)* **13**, 155–160 (1995).
 35. Essen, L. O., Harrenga, A., Ostermeier, C. & Michel, H. 1.3 Å X-ray structure of an antibody Fv fragment used for induced membrane-protein crystallization. *Acta. Crystallogr. D. Biol. Crystallogr.* **59**, 677–687 (2003).
 36. Ritchie, T. K. et al. Chapter 11 - Reconstitution of membrane proteins in phospholipid bilayer nanodiscs. *Methods Enzymol.* **464**, 211–231 (2009).
 37. Zivanov, J. et al. New tools for automated high-resolution cryo-EM structure determination in RELION-3. *Elife* **7**, <https://doi.org/10.7554/eLife.42166> (2018).
 38. Zivanov, J., Nakane, T. & Scheres, S. H. W. Estimation of high-order aberrations and anisotropic magnification from cryo-EM data sets in RELION-3.1. *IUCr. J.* **7**, 253–267 (2020).
 39. Zheng, S. Q. et al. MotionCor2: Anisotropic correction of beam-induced motion for improved cryo-electron microscopy. *Nat. Methods* **14**, 331–332 (2017).
 40. Rohou, A. & Grigorieff, N. CTFIND4: Fast and accurate defocus estimation from electron micrographs. *J. Struct. Biol.* **192**, 216–221 (2015).
 41. Terwilliger, T. C., Ludtke, S. J., Read, R. J., Adams, P. D. & Afonine, P. V. Improvement of cryo-EM maps by density modification. *Nat. Methods* **17**, 923–927 (2020).
 42. Harrenga, A. & Michel, H. The cytochrome c oxidase from *Paracoccus denitrificans* does not change the metal center ligation upon reduction. *J. Biol. Chem.* **274**, 33296–33299 (1999).
 43. Adams, P. D. et al. PHENIX: A comprehensive Python-based system for macromolecular structure solution. *Acta. Crystallogr. D. Biol. Crystallogr.* **66**, 213–221 (2010).
 44. Chen, V. B. et al. MolProbity: All-atom structure validation for macromolecular crystallography. *Acta. Crystallogr. D. Biol. Crystallogr.* **66**, 12–21 (2010).
 45. Pettersen, E. F. et al. UCSF Chimera—a visualization system for exploratory research and analysis. *J. Comput. Chem.* **25**, 1605–1612 (2004).
 46. Goddard, T. D. et al. UCSF ChimeraX: Meeting modern challenges in visualization and analysis. *Protein Sci.* **27**, 14–25 (2018).

Acknowledgements

We would like to thank Susann Kaltwasser and Norbert Zint for their technical assistance. This work was supported by the Max Planck Society, the Nobel laureate Fellowship programme of the Max Planck Society (to SS) and the Deutsche Forschungsgemeinschaft (Cluster of Excellence, Macromolecular Complexes Frankfurt).

Author contributions

F.K. designed experiments, purified aa₃ oxidase and Fv fragment, performed nanodisc reconstitution, performed spectroscopic measurements, collected cryo-EM data, processed cryo-EM data, refined the structures, built the model, drafted the paper and prepared figures. S.S. prepared grids, collected cryo-EM data, refined the structures and drafted the paper. Z.P. and H.M. purified aa₃ oxidase, Fv fragment and nanodiscs. S.W. aligned the microscope and collected cryo-EM data. H.M. supervised the project, interpreted results and rewrote the paper.

Funding

Open Access funding enabled and organized by Projekt DEAL.

Competing interests

The authors declare no competing interests.

Additional information

Supplementary information The online version contains supplementary material available at <https://doi.org/10.1038/s41467-021-27174-y>.

Correspondence and requests for materials should be addressed to H. Michel.

Peer review information *Nature Communications* thanks the anonymous reviewers for their contribution to the peer review of this work.

Reprints and permission information is available at <http://www.nature.com/reprints>

Publisher's note Springer Nature remains neutral with regard to jurisdictional claims in published maps and institutional affiliations.



Open Access This article is licensed under a Creative Commons Attribution 4.0 International License, which permits use, sharing, adaptation, distribution and reproduction in any medium or format, as long as you give appropriate credit to the original author(s) and the source, provide a link to the Creative Commons license, and indicate if changes were made. The images or other third party material in this article are included in the article's Creative Commons license, unless indicated otherwise in a credit line to the material. If material is not included in the article's Creative Commons license and your intended use is not permitted by statutory regulation or exceeds the permitted use, you will need to obtain permission directly from the copyright holder. To view a copy of this license, visit <http://creativecommons.org/licenses/by/4.0/>.

© The Author(s) 2021